The Barriers in the Bimolecular and Unimolecular Folding Reactions of the Dimeric Core Domain of *Escherichia coli Trp* Repressor Are Dominated by Enthalpic Contributions†

Lisa M. Gloss‡ and C. Robert Matthews*

Department of Chemistry and Center for Biomolecular Structure and Function, Pennsylvania State University, University Park, Pennsylvania 16802

Received July 15, 1998; Revised Manuscript Received September 8, 1998

ABSTRACT: The kinetic folding mechanism of the isolated dimerization domain of *E. coli Trp* repressor, $[2-66]_2$ TR, consists of a nearly diffusion-limited association reaction to form a dimeric intermediate, I_2, which is then converted to the native, folded dimeric species, N_2 by a first-order folding step (preceding paper in this issue). The two transition states traversed in the folding of $[2-66]_2$ TR were characterized by monitoring the folding and unfolding reactions by stopped-flow fluorescence as a function of temperature and urea. For both transition states, the barriers are dominated by the enthalpic component; the entropic component accelerates the association reaction but has little effect on the subsequent rearrangement reaction. The transition state between I_2 and N_2 is relatively nativelike, as determined by the sensitivity of the rate constants to denaturant. This study also highlights the key role of solvent entropy in determining the magnitude of the relative free energy of the transition states and the ground states. The positive entropy change for the I_2 to N_2 reaction, presumably arising from the release of solvent from hydrophobic surfaces, is the driving force for this final folding step, offsetting an unfavorable enthalpic term.

A commonly used strategy for understanding how the three-dimensional structure of a protein is encoded by its amino acid sequence is to examine the structure, stability, and dynamics of partially folded forms that appear during folding reactions (*1*, *2*). Transiently populated species and exponential responses that describe their formation and decay are observed in the folding of many proteins, implying that substantial barriers exist on the energy surface that describes a protein folding reaction. Characterization of the transition states that link intermediates to the native and unfolded forms provides additional insights into the protein folding code.

By monitoring the temperature dependence of the folding and/or unfolding reactions, the thermodynamic properties of the transition states can be ascertained. Transition-state analyses have been reported for a number of monomeric proteins, for example: T4 lysozyme (*3*), the α subunit of tryptophan synthase, αTS[1] (*4*), chymotrypsin inhibitor 2 and barnase (*5*−*7*), cold-shock protein B (8), the Fyn-SH3 domain (*9*), the N-terminal domain of phosphoglycerate kinase, and the domain 1 of the T-cell adhesion protein CD2 (*10*). A common feature of the temperature dependence of the folding and unfolding reactions of these proteins is curvature in the plots of $\ln(k_{obs})$ vs $1/T$, rather than a linear dependence as would be expected for a simple Arrhenius model. Nonlinear behavior is consistent with a substantial change in heat capacity and is usually attributed to the burial of a hydrophobic surface in the folding reaction (*3*). Another common feature of the barriers in folding/unfolding reactions is that they are generally dominated by an enthalpic component, with $\Delta H^{\circ\ddagger}$ values of 8−24 kcal mol^{-1}. In contrast, the entropic contributions to transition states vary considerably from protein to protein. Both positive and negative values have been reported; the sign presumably reflects whether the contribution of the conformational entropy (negative upon folding) or solvent entropy (positive upon folding) is more substantial.

The transition-state analysis of the association reaction in the folding of the dimeric protein, P-22 Arc repressor, has also been reported (*11*). The single transition state detected for this system involves formation not only of secondary and tertiary structure but also the development of quaternary structure. Like the monomeric systems, the transition state of P-22 *Arc* repressor exhibits a substantial change in heat capacity and a dominating enthalpic component. The net entropic contribution to the transition state of P-22 Arc is insignificant, despite the reduction in the molecularity of the system. Further characterizations of the transition states in dimeric folding reactions are required to test the generality of these observations and to enhance the comparison with monomeric folding reactions.

This paper reports the transition-state analysis of another dimeric model system, the *E. coli Trp* repressor (TR[1]) dimerization domain, $[2-66]_2$ TR. Full-length TR is a prototypical member of the helix-turn-helix family of DNA-binding proteins. Each monomer of 107 residues contains six α-helices (*12*, *13*). The A−C helices of each monomer

† Supported by National Institutes of Health (NIH) Grant GM 54836 to C.R.M. L.M.G. was supported in part by an NIH Postdoctoral Fellowship GM 16685.

* To whom correspondence should be addressed.

‡ Present address: Department of Biochemistry and Biophysics, Washington State University, Pullman, WA 99164-4660.

10.1021/bi981694f CCC: $15.00
Published on Web 10/23/1998

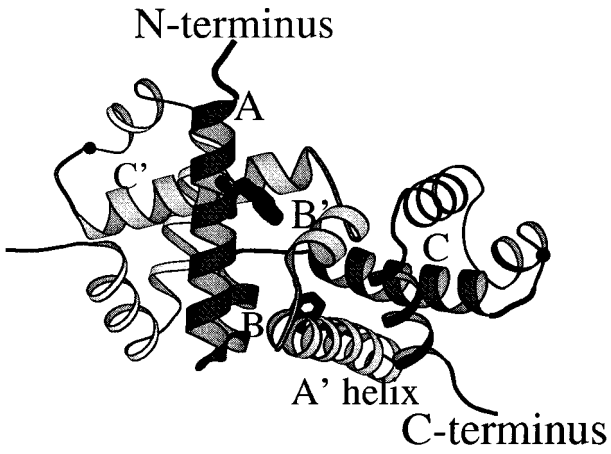

FIGURE 1: Ribbon diagram of full-length WT *Trp* repressor from the X-ray crystal structure (*12*). The $[2-66]_2$ TR variant spans helices A, B, C, A′, B′, and C′, shown in the wider ribbons; the terminal residues, 66 and 66′, are indicated by the black spheres. The single tryptophan remaining in core fragment, Trp-19, is shown. This figure was generated using Molscript v1.4 (*51*).

form the hydrophobic core and dimerization domain of TR; these three helices from each monomer are intertwined in a topologically complex interface (Figure 1). A fragment that contains the dimerization core, spanning residues 2−66, has been constructed by stop codon mutagenesis (*14*).

The equilibrium folding responses of WT TR and $[2-66]_2$ TR, reversibly induced by urea, are two-state processes (*14*, *15*). However, the proposed kinetic mechanism for the folding of full-length WT TR is very complex (*16*); there appear to be three parallel folding channels through which the unfolded monomer can fold to the native dimer. Each channel contains a burst-phase monomeric intermediate and dimerization and nonproline isomerization reactions. A detailed analysis of the transition states in such a complicated mechanism is practically impossible.

Fortunately, $[2-66]_2$ TR folds by a much simpler set of reactions (preceding paper in this issue). The kinetic folding mechanism of this dimeric autonomous folding unit is well-described by a nearly diffusion-limited association reaction to form a dimeric intermediate, I_2. This intermediate is then converted to the native, folded dimeric species, N_2 by a first-order folding step (Scheme 1).

Scheme 1

$$2\,U \underset{k_{IU}}{\overset{k_{UI}}{\rightleftharpoons}} I_2 \underset{k_{NI}}{\overset{k_{IN}}{\rightleftharpoons}} N_2$$

The simplicity of this reaction permits detailed investigation of the thermodynamic properties of a bimolecular association reaction and a unimolecular rearrangement reaction. This paper analyzes the transition states for both the bi- and unimolecular steps, providing insights into the interplay between the enthalpy and entropy changes that govern the folding reactions of multimeric proteins.

MATERIALS AND METHODS

Materials. Ultrapure urea was purchased from ICN Biomedicals Inc. All other chemicals were of reagent grade. The expression and purification of the $[2-66]_2$ TR fragment has been described elsewhere (*14*).

Methods. (a) Stopped-Flow Fluorescence Spectroscopy. The buffer conditions for the kinetic folding experiments were 10 mM potassium phosphate, 0.1 mM EDTA, pH 7.6, with varying concentrations of ultrapure urea. SF-FL traces with final monomer concentrations of 7 μM monomer were collected using a BioLogic SFM-3 stopped-flow module interfaced with the BioLogic light source and detection unit. The dead time of the BioLogic SF instrument was ∼5 ms, with cuvette path lengths of 1.5 and 2 mm. The excitation wavelength was 295 nm with a 9 nm bandwidth and emission detected after a 320 nm cutoff filter. Using two channels for data collection, fluorescence intensity data were collected over two time ranges: 1 s data (Δt = 1 ms) with an instrumental time constant of 1 ms and 2−10 s (Δt = 2−10 ms) with an instrumental time constant of 2−5 ms. The signal-to-noise ratio was enhanced by averaging 4−10 shots per typical SF-FL trace.

To collect SF-FL data at sub-micromolar monomer concentrations, an Applied Photophysics SFM 17 MV stopped-flow instrument was used. The dead time was ∼6 ms with a path length of 2 mm. The excitation wavelength was 285 nm with a 9.3 nm bandwidth. Four to six shots were averaged per kinetic trace.

(b) Data Collection and Analysis. To monitor the dimerization reaction in the folding of $[2-66]_2$ TR, SF-FL data were collected at 0.2−0.4 μM monomer, at temperatures between 7 and 17 °C. The final urea concentration was 1.0 M. The SF-FL unfolding and refolding traces were also collected at 7 μM monomer, where only the $I_2 \rightleftharpoons N_2$ reaction can be monitored (Scheme 1). At this higher concentration, refolding data were collected over a temperature range from 5 to 35 °C and urea concentrations from 0.75 to 2.0 M (at 2.5 °C and 0.25 M intervals, respectively). The unfolding reaction was monitored from 10 to 35 °C and from 5.25 to 7.0 M urea, with the same intervals as the refolding data. Unfolding data could not be collected below 10 °C at all urea concentrations due to the limited solubility of urea. Two matrices of temperature/urea conditions were obtained, 94 points for unfolding, 65 for refolding, with at least three SF-FL traces for each condition.

Individual kinetic traces were fit locally, with identical results, using either the Macintosh version of KaleidaGraph 3.0 (Abelbeck Software) or an in-house fitting routine, Savuka 5.0 (*17*), to an equation of an exponential form:

$$F(t) = F_\infty + \sum_{i=1}^{N} \Delta F_i \exp(-k_i t) \qquad (1)$$

where F_∞ is the fluorescence signal at infinite time and ΔF_i is the fluorescence change associated with the kinetic phase described by the rate constant, k_i. SF-FL data at 7 μM monomer were well-described by local fits to a single-

[1] Abbreviations: $[2-66]_2$ TR, dimeric *Trp* repressor fragment containing residues 2−66; [2−66] TR, monomeric species of $[2-66]_2$ TR.; αTS, alpha subunit of tryptophan synthase; CD, circular dichroism; ΔASA, change in solvent accessible surface area; F_{app}, apparent fractional population of a species in the folding reaction; FL, fluorescence; k_{XY}, the rate constant for the transformation of X to Y.; $\Delta Z^{\circ\ddagger}$, where Z is one of the thermodynamic properties, H (enthalpy), S (entropy), G (Gibbs free energy), or ΔC_p (heat capacity), the thermodynamic properties of the transition state for the reaction of X to Y, as noted by attached subscripts; SF, stopped-flow; TR, *Trp* aporepressor; WT, dimeric wild-type *Trp* aporepressor containing residues 2−108.

exponential term, with rate constants for k_{IN} or k_{NI} (Scheme 1). The Savuka 5.0 program was used for globally fitting data sets as a function of temperature or urea, as described in Results.

At sub-micromolar monomer concentrations, the refolding kinetic response of $[2-66]_2$ TR required fitting to two kinetic phases to describe the SF-FL traces with k_{IN} as the first-order rate constant and k_{UI} is the second-order rate constant (Scheme 1). Data at a given temperature were fit globally to the differential equations describing second- and first-order rate constants in a sequential set of reactions by numerical methods (*18*, *19*); the equations included the values of the unfolding rate constants (k_{IU} and k_{NI}). In this analysis, data at three monomer concentrations were used: 0.1, 0.2, and 0.4 μM or 0.2, 0.3, and 0.4 μM monomer. Under conditions of small perturbations, the expression for a second-order reaction can be reduced to an exponential form (*20*). At the sub-micromolar concentrations used and 1 M urea, the change in F_{app} for I_2 is $\leq$30% (calculated from a $\Delta G°(H_2O) = 10.3$ kcal mol^{-1} for a standard state of 1 M monomer and an m value of 1.2 kcal mol^{-1} M^{-1}; preceding paper in this issue). When the data at 0.2 and 0.4 μM monomer were fit globally as a function of temperature, a sum of two exponentials were used to approximate the values for k_{UI} and k_{IN}. This equation requires fewer parameters than obtaining numerical solutions to the differential equations necessary to describe the kinetic mechanism of Scheme 1.

RESULTS

$[2-66]_2$ TR contains one tryptophan per monomer, Trp-19, which is completely buried in the dimer interface (Figure 1), and makes several interdimer contacts in the folded form of WT TR (*12*, *13*). The intrinsic tryptophan fluorescence response, monitored by SF-FL, for both the folding and unfolding reactions, monitors the development of tertiary and quaternary structure; the kinetics determined by SF-FL are similar to that seen by SF-CD, which monitors the development of secondary structure (preceding paper in this issue). However, the much larger signal-to-noise ratio of SF-FL permits direct detection of the very rapid $2U \rightarrow I_2$ reaction. Therefore, rapid mixing fluorescence techniques were used exclusively to monitor the folding and unfolding reactions of $[2-66]_2$ TR as a function of temperature and urea in the present study.

In refolding jumps, at temperatures below 20 °C and sub-micromolar monomer concentrations, a second-order reaction for the dimerization of [2−66] TR monomers can be detected by SF-FL (Figure 4 of the preceding paper in this issue). When the data are fitted globally as a function of monomer concentration, an association rate constant can be determined; at 1.0 M urea, from 7 to 17 °C, this rate is on the order of 10^8 M^{-1} s^{-1} (preceding paper in this issue).

Thermodynamic Properties of the Transition State of the $2U \rightarrow I_2$ Reaction. The temperature dependence of the second-order rate constant was examined by global fitting of the SF-FL data collected at 0.2 and 0.4 μM monomer, over a temperature range of 7 to 17 °C. A set of 27 traces was fitted to eq 1 with an Arrhenius description of the rate constants:

$$\ln(k_i) = \ln(A_i) - E_{a,i}/RT \qquad (2)$$

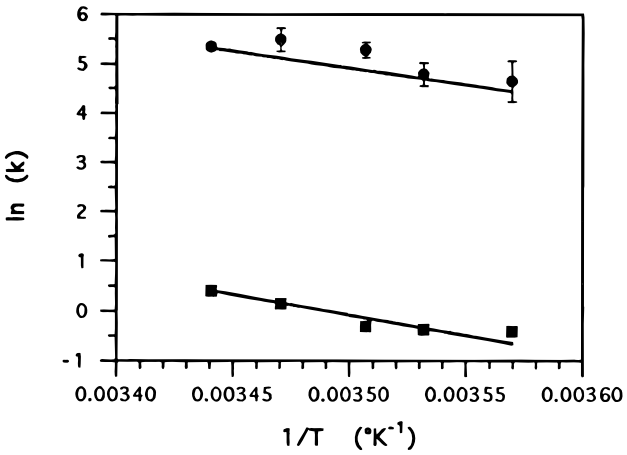

FIGURE 2: Temperature dependence of the second-(circles) and first-order (squares) folding reactions of $[2-66]_2$ TR. Stopped-flow fluorescence data were collected at 0.2 and 0.4 μM monomer at 7, 10, 12, 15, and 17 °C. The observed rates, from local fits to a $2U \rightarrow I_2 \rightarrow N_2$ model, are represented by the data points. The solid lines represent the global fits of the data, using an Arrhenius-type parametrization of the temperature dependence (eq 2). Conditions: 1 M urea, 10 mM potassium phosphate, 0.1 mM EDTA, pH 7.6.

The values of $\ln(A_i)$ for the second-order reactions were linked only for data collected at the same monomer concentration; for the first-order reactions, the value of $\ln(A_i)$ was either linked only within a given monomer concentration or linked globally over both monomer concentrations, with similar results. The values of E_a were treated as global parameters for all monomer concentrations. The results are shown in Figure 2. For comparison, the values of k_{UI} and k_{IN} from local fits to the model shown in Scheme 1, in which the differential equations describing the first- and second-order rate constants were solved by numerical methods (*19*), are also shown. The global fits, using a sum of two exponentials are in excellent agreement with local fits employing the more precise differential equations for describing a second-order reaction (*18*, *20*).

The global analysis of the data yielded an E_a value of 13.5 $\pm$ 0.1 for the second-order rate constant. The value of E_a can be used to predict a rate constant at 25 °C and 1 M urea of 7×10^8 M^{-1} s^{-1} for the $2U \rightarrow I_2$ reaction. Since in solution and at constant pressure $E_a = \Delta H°^{\ddagger} + RT$ (*21*), $\Delta H°^{\ddagger}$ is estimated to be 12.9 kcal mol^{-1} under these conditions (Table 1).

Estimates of $\Delta G°^{\ddagger}$ and $\Delta S°^{\ddagger}$ depend on the relationship between the observed rate constant and $\Delta G°^{\ddagger}$. Transition-state theories postulate that

$$k_{obs} = k_a \exp\left(\frac{-\Delta G°^{\ddagger}}{RT}\right) = k_a \exp\left(\frac{-\Delta H°^{\ddagger}}{RT}\right) \exp\left(\frac{\Delta S°^{\ddagger}}{R}\right) \qquad (3)$$

though there are different definitions of the preexponential term. In the Eyring formalism (*22*), $k_a = k_B T/h$, where k_B and h are the Boltzmann and Planck constants, respectively. In the Kramers formalism (*23*), $k_a = \kappa_0/\eta$, where κ_0 is the rate constant in the absence of a barrier and η is the solvent viscosity. Although the Eyring equation has often been employed to relate kinetic and thermodynamic parameters in monomeric protein folding reactions (e.g. refs *3*−*10* and *24*), the Kramers model is particularly appropriate for an association reaction in solution. For a diffusion-controlled,

Table 1: Thermodynamic Parameters Describing the Transition States of the Folding Reactions of $[2-66]_2$ TR[a]

reacn and formalism	$\Delta H^{\circ\ddagger}$ (kcal mol^{-1})	$\Delta S^{\circ\ddagger}$ (cal mol^{-1} K^{-1})	$\Delta C_p^{\circ\ddagger}$ (cal mol^{-1} K^{-1})	$\Delta G^{\circ\ddagger}$ (kcal mol^{-1})
$2U \rightarrow I_2$[a]				
Kramers	12.9 (0.1)	40	ND	0.9
Eyring	12.9 (0.1)	25.2	ND	5.4
$I_2 \rightarrow N_2$[b]				
Kramers	18.8 (0.7)	32 (4)	−290 (50)	9.7 (0.4)
Eyring	18.8 (0.7)	14 (2)	−290 (50)	15.3 (0.6)
$N_2 \rightarrow I_2$[c]				
Kramers	16.56 (0.08)	15.6 (0.4)	396 (3)	11.9 (0.3)
Eyring	16.56 (0.08)	−3.17 (0.08)	396 (3)	17.5 (0.4)

[a] $T^\circ = 298$ K. Standard deviations are given in parentheses. [b] The $\Delta H^{\circ\ddagger}$ value is from global fitting of data in Figure 2 to an Arrhenius temperature dependence (eq 2). The values of $\Delta G^{\circ\ddagger}$ and $\Delta S^{\circ\ddagger}$ are dependent on the formalism employed to relate the rate constant to the activation energy; they have been calculated setting $k_a = 3.3 \times 10^9$ M^{-1} s^{-1} and $k_a = k_B T/h = 6.2 \times 10^{12}$ s^{-1}, as in the Kramers and Eyring formalisms, respectively. [c] The temperature dependence of all the SF-FL traces at a given urea concentration (from 0.75 to 2.0 M urea) were globally fitted to eqs 6 and 7. There was no discernible urea dependence for $\Delta C_p^{\circ\ddagger}$. The values of $\Delta H^{\circ\ddagger}$, $\Delta S^{\circ\ddagger}$, and $\Delta G^{\circ\ddagger}$ are derived from a linear dependence of the parameter on urea concentration and represent the predicted value in the absence of urea. The values of $\Delta G^{\circ\ddagger}$ and $\Delta S^{\circ\ddagger}$ were determined using the k_a of the Eyring formalism and $k_a = 5 \times 10^8$ s^{-1} from the Kramers formalism. [d] All of the SF-FL data in a matrix of 94 urea and temperature conditions were globally fitted to eqs 6 and 7. The values of $\Delta S^{\circ\ddagger}$ or $\Delta C_p^{\circ\ddagger}$ were treated as global parameters independent of urea concentration. The value of $\Delta H^{\circ\ddagger}$ was allowed to vary with the urea concentration. The $\Delta H^{\circ\ddagger}$ and $\Delta G^{\circ\ddagger}$ values represent linear extrapolations of values to 0 M urea. The k_a values are the same as those used for the first-order folding reaction.

second-order reaction, a theoretical maximal rate constant can be calculated to substitute for κ_0/η in the Kramers equation. In a diffusion−collision model, the diffusing monomers are represented as spheres with uniformly reactive surfaces with no electrostatic component to their interaction (*20*, *25*). The upper limit of the rate constant for the diffusion-limited association of a dimeric system, in the absence of a barrier, can be obtained using the Einstein−Smoluchowski relationship:

$$k_a/(\mathrm{M}^{-1}\,\mathrm{s}^{-1}) = \frac{4RT}{3\eta} \tag{4}$$

This equation reflects the fact that the rate constant for a homodimeric association reaction is half that of a heterodimeric reaction (*20*). This yields a value of $\sim 3.3 \times 10^9$ M^{-1} s^{-1} for a homodimer, at 25 °C in aqueous solution (*26*). The inclusion of an attractive electrostatic component would enhance the theoretical maximal association rate. However, the association of WT TR is unaffected by ionic strength, suggesting that electrostatic interactions are not important in the association of TR monomers (*52*).

Using $k_a = 3.3 \times 10^9$ M^{-1} s^{-1} in eq 3, and the $\Delta H^{\circ\ddagger}$ value estimated from the data in Figure 2, the values of $\Delta S^{\circ\ddagger}$ and $\Delta G^{\circ\ddagger}$ at 1 M urea are estimated to be 40 cal mol^{-1} K^{-1} and 0.92 kcal mol^{-1}, respectively (Table 1). The Eyring formalism reflects an extreme upper limit for the value of k_a, and Table 1 also shows the $\Delta S^{\circ\ddagger}$ and $\Delta G^{\circ\ddagger}$ values calculated using a preexponential factor of $k_B T/h$. The ∼1000-fold higher value of k_a increases the value of $\Delta G^{\circ\ddagger}$ to 5.4 kcal mol^{-1} and decreases the $\Delta S^{\circ\ddagger}$ term to 25.2 cal mol^{-1} K^{-1}.

Unfortunately, the limited temperature range over which data could be collected prevented any meaningful fitting of the data to a more complicated model that explicitly recognizes the contribution of $\Delta C_p^{\circ\ddagger}$ to the activation enthalpy and entropy (such as in eqs 6 and 7 as follow).

Thermodynamic Properties of the Transition State between the I_2 and N_2 Species. (a) Analysis. To monitor the $I_2 \rightleftharpoons N_2$ folding and unfolding reactions, data were collected at 7 μM monomer, where the preceding second-order folding reaction is complete in the stopped-flow dead time. For both the folding and unfolding reactions, data were collected not only as a function of temperature but also as a function of urea, resulting in a matrix of urea/temperature conditions. This permits the determination of the urea dependence, if any, of the thermodynamic properties of the transition state, and the extrapolation of these properties to a standard state of 0 M urea. The data were analyzed by both axes of the matrix, i.e. as a function of urea at a given temperature and as a function of temperature at a given urea concentration.

The urea dependence of the folding or unfolding rates, at a particular temperature, was globally fitted to the equation:

$$k_i = k_i(\mathrm{H_2O}) \exp\left(\frac{-m_i^{\ddagger}[\mathrm{Urea}]}{RT}\right) \tag{5}$$

where $k_i(H_2O)$ is the rate constant of the folding or unfolding reaction in the absence of urea and $m_i^{\ddagger}$ reflects the sensitivity of the reaction to denaturant. Equation 5 was also used to describe the urea dependence of k_{IN} and k_{NI} from the local fits of the data to eq 1.

The temperature dependence, at a given final urea concentration, was parametrized according to the Eyring formalism (*3*, *4*, *27*) in the following manner:

$$\ln(k_i/T) = A + B(T^\circ/T) + C\ln(T^\circ/T) \tag{6}$$

where T° was chosen as 298 K, and $A-C$ are defined by thermodynamic parameters as

$$A = \frac{\Delta S^{\circ\ddagger}(T^\circ) - \Delta C_p^{\circ\ddagger}}{R} + \ln\left(\frac{k_B}{h}\right) \tag{7a}$$

$$B = \frac{\Delta C_p^{\circ\ddagger} - \Delta H^{\circ\ddagger}(T^\circ)/T^\circ}{R} \tag{7b}$$

$$C = \frac{-\Delta C_p^{\circ\ddagger}}{R} \tag{7c}$$

Equations 6 and 7 were used to extract thermodynamic parameters for the transition states of the $I_2 \rightleftharpoons N_2$ reactions from the rates determined from local fits to eq 1, as well as to fit globally SF-FL traces at several temperatures and a particular urea concentration. In global analyses, using either

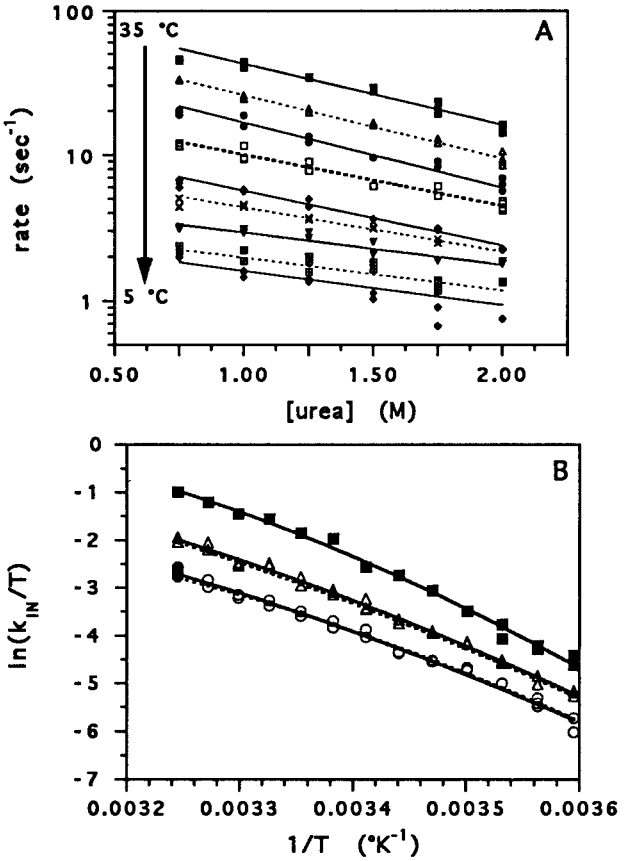

FIGURE 3: Urea and temperature dependence of the first-order refolding reaction of $[2-66]_2$ TR monitored by stopped-flow fluorescence. (A) Urea dependence of $[2-66]_2$ TR folding reactions. The data points represent the local fits of the kinetic traces to a single exponential. Data were collected at 2.5 °C intervals from 35 to 5 °C; for clarity, only the data at 35, 30, 25, 20, 15, 12.5, 10, 7.5, and 5 °C are shown. The lines represent the global fits of the data at a given temperature to eq 5. (B) Temperature dependence of the folding reactions of $[2-66]_2$ TR collected at every 0.25 M urea from 0.75 to 2 M. The values of k_{IN} (H_2O) (■) were determined from the global fits of the data in panel A to eq 5. Representative local fits to a single exponential are also shown, at 1.0 and 1.75 M urea (Δ and ○, respectively). The solid lines represent fits of the data points to the Eyring equation (eq 6). The dashed lines for the 1.0 and 1.75 M data are the results of global fitting of the data at a single urea concentration to eq 6. Conditions: 7 μM monomer, 10 mM potassium phosphate, 0.1 mM EDTA, pH 7.6.

eq 5 or 6, the spectral properties of the I_2 and N_2 species (related to the terms F_∞ and ΔF_i in eq 1) were treated as local fitting parameters for each kinetic trace.

(b) I_2 to the Transition State—Refolding Reaction. A subset of the locally fitted values of k_{IN} for the first-order refolding reaction is shown, plotted as a function of urea and temperature, in Figure 3A,B, respectively. The lines in Figure 3A represent the global fits of the data, at a given temperature, to eq 5. When the observed rates are plotted as a function of urea concentration, an exponential dependence is observed, described by a single $m^\ddagger$ value (eq 5). This simple response is consistent with a single reaction converting I_2 to N_2, with no additional dimeric intermediates. While a single $m^\ddagger$ value describes the urea dependence of k_{IN} at a given temperature, from 5 to 35 °C, there is a significant temperature dependence of the $m^\ddagger$ values for this reaction (Figure 4). The $m^\ddagger$ value ranges from 0.29 kcal mol^{-1} M^{-1} at 5−10 °C to 0.61 kcal mol^{-1} M^{-1} at 25−35 °C. When the values of $\ln(k_{IN}/T)$ are plotted as a function of $1/T$ (Figure 3B), a small but significant curvature is seen. Nonlinearity in such plots has been attributed to a change in buried surface area and a significant value of $\Delta C_p^{\circ\ddagger}$ (e.g. refs *3*−*10*).

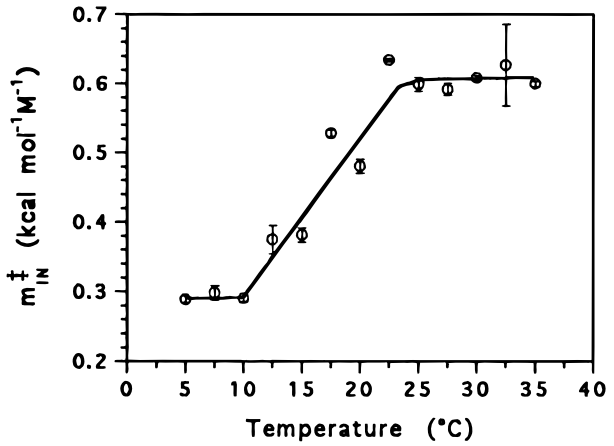

FIGURE 4: Temperature dependence of the $m^\ddagger$ value for the folding reaction. The values were obtained from global fits of the data at a given temperature to eq 5. The line is drawn to guide the eye.

The data were fitted using three strategies to compare the results of local and global fits. (1) Each kinetic trace was fitted individually to a single exponential, and the observed values of k_{IN} at a given urea concentration were then fit to eqs 6 and 7 to describe the temperature dependence of the local fits. (2) Kinetic traces at several urea concentrations and a given temperature were fitted to eq 5. This yielded values of $k_{IN}(H_2O)$ as a function of temperature, which were then fitted to eqs 6 and 7 to obtain values of $\Delta H^{\circ\ddagger}$, $\Delta S^{\circ\ddagger}$, $\Delta G^{\circ\ddagger}$ and $\Delta C_p^{\circ\ddagger}$ in the absence of urea. (3) Kinetic traces collected from 5 to 35 °C and a given urea concentration were globally fitted to eqs 6 and 7. The results of these three fitting methods are in good agreement and are shown in Figure 5.

The results of the global fits are shown in Table 1 and represent the thermodynamic parameters in the absence of urea. The enthalpic contribution to the barrier is large and positive, 18.8 kcal mol^{-1}. The values of $\Delta S^{\circ\ddagger}$ and $\Delta G^{\circ\ddagger}$ are given using a k_a valued derived from both the Eyring and Kramers formalisms; for the latter, a value of 5×10^8 s^{-1} was used for κ_0/η, based on model peptide data (*28*, *29*). The values for $\Delta S^{\circ\ddagger}$ and $\Delta G^{\circ\ddagger}$ range from 14 to 32 cal mol^{-1} K^{-1} and from 10 to 15 kcal mol^{-1}, respectively.

When the data are fit as a function of temperature or urea (method 1 or 3 above), there is a clear linear dependence of $\Delta S^{\circ\ddagger}$ and $\Delta H^{\circ\ddagger}$, and thus $\Delta G^{\circ\ddagger}$ on urea concentration (Figure 5). The slopes describing the linear urea dependence of $\Delta S^{\circ\ddagger}$, $\Delta H^{\circ\ddagger}$ and $\Delta G^{\circ\ddagger}$ are −9 cal mol^{-1} K^{-1} M^{-1}, −1.9 kcal mol^{-1} M^{-1}, and 0.54 kcal mol^{-1} M^{-1}, respectively. The $\Delta C_p^{\circ\ddagger}$ between I_2 and the transition state appears to be independent of denaturant concentration (data not shown).

In the absence of urea at 25 °C, the value of $\Delta G^{\circ\ddagger}$ is determined largely by the magnitude of $\Delta H^{\circ\ddagger}$. The entropic contribution decreases the free energy barrier between I_2 and N_2, though not as greatly as seen for the $2U \rightarrow I_2$ reaction. There is a significant burial of surface area between I_2 and the transition state, corresponding to a $\Delta C_p^{\circ\ddagger}$ value of −0.3 kcal mol^{-1} K^{-1} (Table 1).

(c) N_2 to the Transition State—Unfolding Reaction. The values of k_{NI} for the unfolding of N_2, determined from local

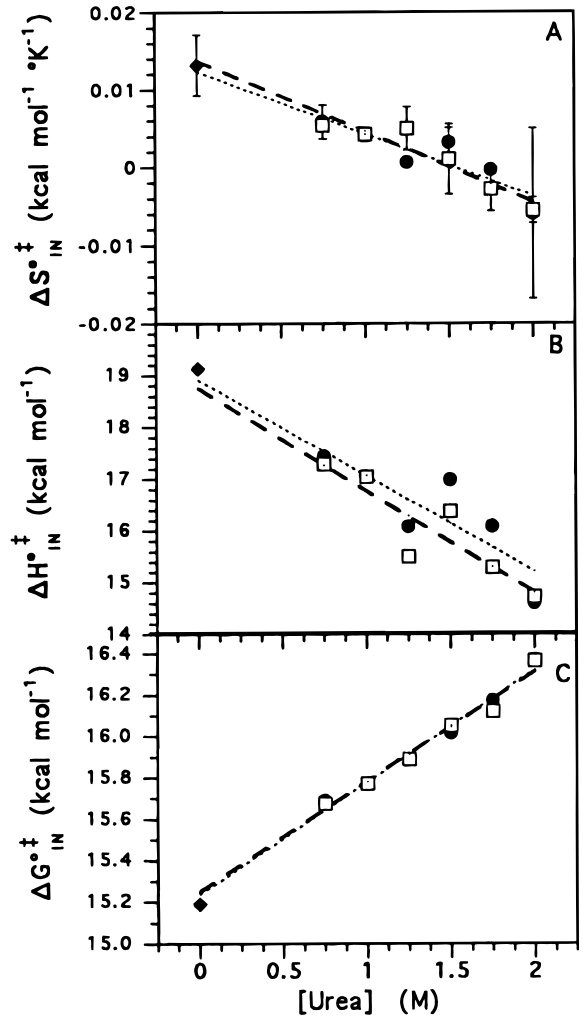

FIGURE 5: Urea dependence of the $\Delta S^{\circ\ddagger}$ (A) and $\Delta H^{\circ\ddagger}$ (B) and $\Delta G^{\circ\ddagger}$ (C) values describing the transition state of the $I_2 \rightarrow N_2$ first-order folding reaction. Key for all panels: ●, traces fit individually to a single exponential and the values of k_{obs} at a single urea concentration fitted to an Eyring temperature dependence (eq 6); ···, linear urea dependence of locally fitted ● data points; □, temperature dependence of all traces at a single urea concentration fit simultaneously to eq 6; --, linear urea dependence of locally fitted □ data points; ♦, value fitted from the temperature dependence of $k_{IN}(H_2O)$. For panel A, errors are shown or are equivalent to the size of the data points. For ease of viewing, error bars are not included in panels B and C; the average error for the ● and ♦ data points are 20−30%. The average error for the globally fitted □ data points is <1% for $\Delta H^{\circ\ddagger}$ and $\Delta G^{\circ\ddagger}$.

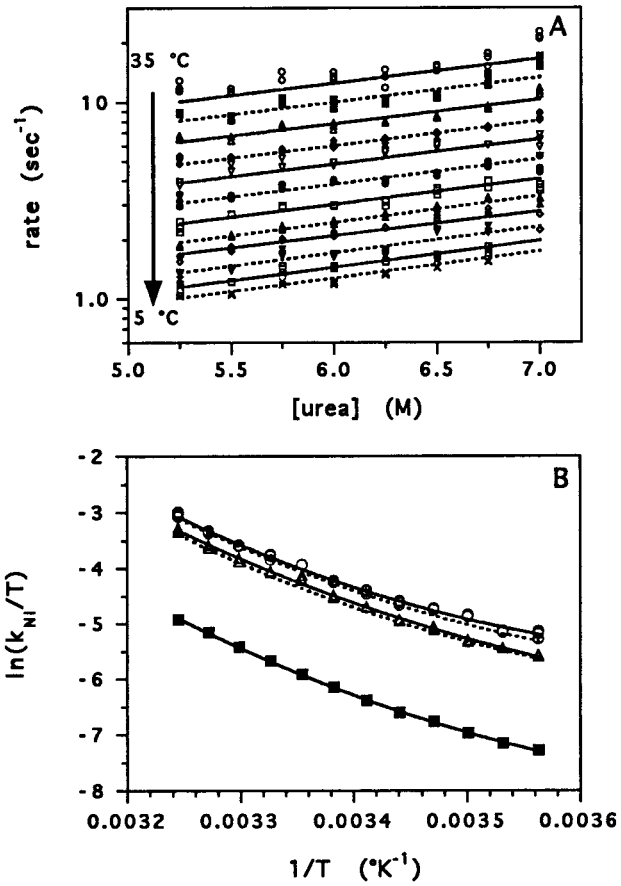

FIGURE 6: Urea and temperature dependence of the unfolding reaction of $[2-66]_2$ TR monitored by stopped-flow fluorescence. (A) Urea dependence of $[2-66]_2$ TR unfolding reaction. The data points represent the local fits of the kinetic traces to a single exponential. Data were collected at 2.5 °C intervals from 35 to 7.5 °C. The lines are the result of global fits of the data to eq 5 as described in the text. (B) Temperature dependence of the unfolding reaction of $[2-66]_2$ TR. The values of $k_{NI}(H_2O)$ (■) were determined from the global fit of the data in panel A to eq 5. Representative unfolding data, locally fit to a single exponential, are also shown, 5.5 and 6.5 M urea (Δ and ○, respectively). The solid lines represent fits of the data points to the Eyring equation (eq 6). The dashed lines for the 5.5 and 6.5 M data are the results of global fitting of all the data (5.25−7.0 M urea) simultaneously to eq 6. Conditions are given in caption of Figure 3.

fits of SF-FL traces to a single exponential, are shown as a function of urea in Figure 6A. Like the I_2 to N_2 folding reaction, the k_{NI} values depend on the urea concentration in a simple exponential manner. There is no temperature dependence of the $m^{\ddagger}$ value for this reaction, unlike that seen for the first-order folding reaction. The lines in Figure 6A represent the global fits of the data, at a given temperature, to eq 5, with a global value for $m^{\ddagger}$. The average $m^{\ddagger}$ value, derived from fits of k_{NI} at a single temperature to eq 5, is -0.175 ± 0.03 kcal mol^{-1} M^{-1}; the $m^{\ddagger}$ value determined from global fitting is -0.175 ± 0.001 kcal mol^{-1} M^{-1}. The values of $k_{NI}(H_2O)$ and a subset of locally fitted k_{NI} values are plotted as a function of temperature in Figure 6B. The nonlinear behavior of $\ln(k_{NI}/T)$ as a function of $1/T$ implies a nonzero value for $\Delta C_p^{\circ\ddagger}$. The urea dependence of the thermodynamic properties yielded by the different fitting methods (as described above for the I_2 to N_2 reaction) are shown in Figure 7. The scatter for and error of the data are highest for the 7.0 M data set because of a smaller temperature range over which data could be collected (35 to 12.5 °C) owing to the marginal solubility of the unfolding buffer (9−10 M urea) at low temperatures.

Fitting the data as a function of only temperature or urea shows that there is no urea dependence of $\Delta C_p^{\circ\ddagger}$ (data not shown). There is a small but significant urea dependence for the $\Delta G^{\circ\ddagger}$ values, requiring that there must be a slight urea dependence on the $\Delta H^{\circ\ddagger}$ and/or $\Delta S^{\circ\ddagger}$ values that is obscured by the scatter in the data. To ascertain the urea dependence of the $\Delta H^{\circ\ddagger}$ and/or $\Delta S^{\circ\ddagger}$ terms, the entire matrix of data was fit to eq 6, with $\Delta C_p^{\circ\ddagger}$ globally linked over all urea concentrations; only the $\Delta H^{\circ\ddagger}$ and/or $\Delta S^{\circ\ddagger}$ values were permitted to vary with urea concentration. The most satisfactory fit, as judged by the reduced χ^2 values, was obtained when all of the urea dependence was placed on the $\Delta H^{\circ\ddagger}$ parameter. Forcing the $\Delta S^{\circ\ddagger}$ term to be urea inde-

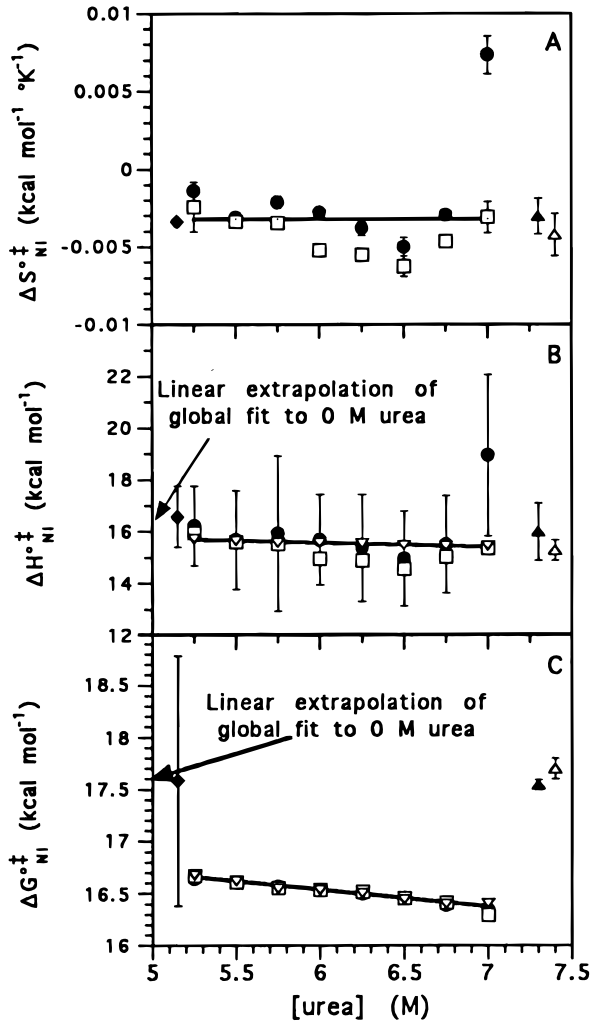

FIGURE 7: Urea dependence of the thermodynamic properties of the transition state in the $N_2 \rightarrow I_2$ unfolding reaction. Errors or standard deviations are shown or are equivalent to the size of the data points. Key for all panels: ● (obscured in panel C), traces fit individually to a single exponential and the values of k_{NI} at a single urea concentration fitted to an Eyring temperature dependence (eq 6 and 7); □, temperature dependence of all traces at a single urea concentration fit simultaneously to eqs 6 and 7; ▲ and Δ, average of the local fits ($\Delta S^{\circ\ddagger}$ and $\Delta H^{\circ\ddagger}$) or linear extrapolation of the local fits to 0 M urea ($\Delta G^{\circ\ddagger}$) for the data represented by the ● and □ symbols, respectively; ♦, value fitted from the temperature dependence of $k_{NI}(H_2O)$ and representing the value at 0 M urea. The data points represented by the ▲, Δ, and ♦ symbols are either urea independent or the values at 0 M urea; they are plotted at arbitrary urea concentrations for comparison purposes only. Panel A: The values of $\Delta S^{\circ\ddagger}$ from the various local and global fitting methods. The solid line represents the value obtained from the global fit of the data at all urea concentrations and temperatures, where $\Delta C_p^{\circ\ddagger}$ and $\Delta S^{\circ\ddagger}$ were treated as urea independent, globally linked parameters. The values of $\Delta H^{\circ\ddagger}$ (B) and $\Delta G^{\circ\ddagger}$ (C) are from the various local and global fitting methods. The results of the global fit of all data (with $\Delta C_p^{\circ\ddagger}$ and $\Delta S^{\circ\ddagger}$ were treated as urea independent, globally linked parameters) are represented by ∇; the solid lines represent the linear urea dependence of global fit. The arrows to the left ordinate represent the value for a linear extrapolation of globally fitted data (∇) to 0 M urea.

pendent did not increase the reduced χ^2 value over that obtained when both thermodynamic parameters were treated as urea dependent. When only the $\Delta S^{\circ\ddagger}$ values were allowed to vary with urea, i.e. $\Delta H^{\circ\ddagger}$ was globally linked and urea independent, the reduced χ^2 value was 3-fold higher than the most satisfactory fit.

The results of the global analysis ($\Delta C_p^{\circ\ddagger}$ and $\Delta S^{\circ\ddagger}$ urea independent) are represented by the solid lines in Figure 7, and presented in Table 1. The values of the $\Delta H^{\circ\ddagger}$ and $\Delta G^{\circ\ddagger}$ parameters, extrapolated to 0 M urea, agree very well with the values obtained from fitting of the $k_{NI}(H_2O)$ data to eq 6 (Figure 7). The results of this global fit for two representative urea concentrations are also shown in Figure 6B; the results of the local and global fits are in good agreement.

The urea dependence of $\Delta H^{\circ\ddagger}$ and $\Delta G^{\circ\ddagger}$ are both −0.16 kcal mol^{-1} M^{-1}. In the absence of urea, the $\Delta H^{\circ\ddagger}$ term, 16.56 kcal mol^{-1}, is the major determinant of the relative free energy of the transition state, 12−18 kcal mol^{-1}, depending on the choice of k_a. The value of $\Delta S^{\circ\ddagger}$ ranges from −3 to +16 cal mol^{-1} K^{-1}.

Thermodynamic Differences and Changes in Solvent Accessible Surface Area between I_2 and N_2. The difference in the thermodynamic properties between N_2 and I_2, at 0 M urea, can be calculated from the data in Table 1 and Figures 5 and 7, given that

$$\Delta Y^{\circ}_{NI} = \Delta Y^{\circ\ddagger}_{NI} - \Delta Y^{\circ\ddagger}_{IN} \quad (8)$$

where Y is the enthalpy, entropy, heat capacity, or Gibbs free energy parameter. Such analyses yield ΔH°_{NI} and ΔS°_{NI} values of −2.3 kcal mol^{-1} and −17 cal mol^{-1} K^{-1}, respectively. Surprisingly, there is a small favorable enthalpy contribution for the unfolding of N_2, but this is more than offset by a large negative value of ΔS°_{NI}. The entropic penalty presumably arises from the hydrophobic effect and the ordering of solvent around hydrophobic surfaces that are exposed in I_2. The free energy difference between N_2 and I_2, 2.3−2.6 kcal mol^{-1}, is in very good agreement with that determined from the urea dependence of folding and unfolding data at 25 °C, 2.5 kcal mol^{-1} (Table 1 of the preceding paper in this issue).

The heat capacity change upon unfolding of N_2 to I_2 is relatively large, ∼700 cal mol^{-1} K^{-1}. From the relationship between ΔC_p° and changes in solvent accessible surface area (ΔASA) (*30*), the ΔC_p° value for the N_2 to I_2 reaction corresponds to ∼4100 Å^2. An *m* value of 0.78 kcal mol^{-1} M^{-1}, previously determined at 25 °C for the N_2 to I_2 reaction (preceding paper in this issue) implies an ΔASA of ∼3700 Å^2 (*30*). The good agreement between these two estimates of ΔASA increases the confidence in the accuracy of the result.

DISCUSSION

Appropriate Models for Thermodynamic Analysis of Transition States in Protein Folding Reactions. The determination of $\Delta G^{\circ\ddagger}$, and thus $\Delta S^{\circ\ddagger}$, depends on the choice of the formalism and its preexponential factor (k_a in eq 3). In contrast, the values of $\Delta H^{\circ\ddagger}$ and $\Delta C_p^{\circ\ddagger}$ are not dependent on the value of k_a (eqs 6 and 7). The most commonly used formalism is that of Eyring, where k_a is assumed to be k_BT/h. However, this equation was derived for a very simple gas-phase reaction, and its applicability to the complicated processes of a protein folding reaction in solution is questionable. The Kramers equation (*23*) is an alternative theory that explicitly quantifies a diffusive component in the free energy barrier, especially pertinent for a second-order association reaction.

Scheme 2

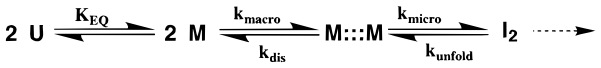

In the application of the Kramers formalism to protein folding, the κ_0 term of the preexponential factor reflects the maximal rate constant for a diffusive reaction in the absence of a barrier (*31*, *32*). For a bimolecular reaction, such as $2U \rightarrow I_2$ for $[2-66]_2$ TR, a plausible estimate for κ_0/η can be calculated from a diffusion−collision model (see Results), yielding a value 3.3×10^9 M^{-1} s^{-1} at 25 °C. However, the appropriate value of κ_0 for an intramolecular folding reaction is unclear; the increase in the local concentration caused by the linking of two chains may enhance the value of κ_0, while excluded volume or chain restriction effects may reduce this value. Experimental results from peptide models for α-helix and β-hairpin formation, as well as the folding of cytochrome *c*, suggest that κ_0 should be in the range of 10^6-10^9 s^{-1} for an intramolecular folding reaction (*28*, *29*, *32*).

Transition State for a Nearly Diffusion-Limited Association Reaction. A purely diffusion-limited association reaction in aqueous solvent, between two identical spherical proteins with uniformly reactive surfaces, should proceed with a rate of 3.3×10^9 M^{-1} s^{-1} (*26*). This rate constant reflects the diffusional macrocollision process of two molecules that are initially far apart in solution. This number is smaller than the total frequency of collisions, including microcollisions, $\sim 10^{11}$ M^{-1} s^{-1} (*20*, *25*). This enhancement reflects the cage effect of a liquid media, which enhances the probability of subsequent collisions after the initial macrocollision. Thus, one could write an expanded mechanism for the dimerization of $[2-66]_2$ TR as shown in Scheme 2, in which a rapid equilibrium between unfolded and folded monomers (U and M, respectively) precedes formation of a loose encounter complex that either disassociates or rearranges/folds to a tighter, more stable complex, I_2.

For WT TR, the monomeric species does fold prior to association (*33*, *34*); a stable monomeric form of [2−66] TR can also adopt helical structure and has an apparent stability of ∼1 kcal mol^{-1} (*53*). The folded monomers of WT TR bind ANS (*33*, *34*), suggesting the presence of hydrophobic surfaces in the M species of Scheme 2. These putative hydrophobic surfaces on folded monomeric [2−66] TR may enhance the rebinding of partially dissociated monomers in the encounter complex, effectively promoting a two-dimensional diffusion of one monomer over the surface of the other. Such a reduction in dimensionality is well-known for the association of DNA-binding proteins and DNA, which has been described as the one-dimensional sliding of cationic proteins along polyanionic DNA (*25*). An analogous phenomena, using hydrophobic surfaces, may be operative in some protein folding reactions.

The broad thermal transition seen for the folding of the full-length TR monomer (*34*) suggests that the enthalpy change for this reaction in [2−66] TR monomers may be a small, negative value. The presumed, rapid preequilibrium (K_{EQ} in Scheme 2) will contribute to the apparent activation enthalpy for the rate-limiting second-order step through its influence on the temperature dependence of the concentration of association-competent monomers, M. The activation enthalpy for a diffusive process, k_{macro} in Scheme 2, should derive predominantly from the friction of water, which is ∼4 kcal mol^{-1} (*35*). Therefore the observed 12.9 kcal mol^{-1} enthalpic barrier for the association of [2−66] TR monomers must reflect a significant, positive contribution from the k_{micro} reaction. The positive value of $\Delta H^{\circ\ddagger}$ for a folding reaction implies that the hydrophobic effect is the dominant determinant of the magnitude of this barrier (*36*).

The $\Delta S^{\circ\ddagger}$ value calculated for the dimerization reaction is substantial and positive, 25−40 cal mol^{-1} K^{-1}, depending on the formalism employed (Table 1). There are three expected contributions to the entropic component of a dimeric protein folding reaction: (1) a decrease in entropy from the loss of side-chain and backbone freedom of ∼6 cal K^{-1} mol-res^{-1} (*37*); (2) an increase in the entropy of the solvent arising from the hydrophobic effect (*38*); and (3) a decrease in entropy from the reduction in molecularity of the system, i.e. two molecules becoming one, that has been estimated to be ∼13−15 kcal mol^{-1} at 298 K (*26*). The favorable $\Delta S^{\circ\ddagger}$ term for the $2U \rightarrow I_2$ reaction suggests that the removal of hydrophobic side chains from the solvent is the major contribution to the magnitude of the entropic component of the transition state.

The activation free energy for the association reaction, 0.9 kcal mol^{-1} or ∼1.5*RT*, is at the lower limit of what is expected for a simple exponential response (*32*, *39*). This result suggests that the estimate for k_a may be too small. A possible enhancement for k_a is a long-range hydrophobic effect, such as that reported for hydrophobic monolayers (*40*, *41*). This behavior would be analogous to the enhancement expected for Coulombic forces and may operate at distances of 10−35 Å.

Comparison with the Transition States of Other Dimeric Folding or Association Reactions. Activation energies have also been measured for other protein folding dimerization reactions that are partially diffusion-controlled. The homodimeric P-22 Arc repressor folds in an apparently two-step process, with a second-order rate constant of 1.4×10^7 M^{-1} s^{-1} at 26 °C (*11*). The $\Delta H^{\circ\ddagger}$ value for this reaction is ∼8 kcal mol^{-1} at 25 °C (calculated from data in Table 1 of ref *11*). The enthalpic contribution to the barrier is lower than that exhibited by $[2-66]_2$ TR; however, the transition state of P-22 Arc contains a much smaller entropy term, 0.2 cal mol^{-1} K^{-1} (employing the Eyring formalism) as compared to ∼30 cal mol^{-1} K^{-1} for $[2-66]_2$ TR. The net result is an activation free energy for folding that is ∼8 kcal mol^{-1}.

The S-peptide of RNase A associates with the folded S protein with a rate of $\sim 2 \times 10^7$ M^{-1} s^{-1} at 25 °C (*42*, *43*). The enthalpy for this transition state, ∼10 kcal mol^{-1}, like those of P-22 Arc and $[2-66]_2$ TR, exceeds that expected for the friction of water by 2- to 3-fold. It is proposed that the RNaseS* association reaction, though its rate approaches the diffusion limit and displays a viscosity effect, is limited by folding (k_{micro} component of Scheme 2) rather than encounter-limited (k_{macro}) (*43*). For the association of [2−66] monomers, which proceeds with a rate constant ∼30 times greater, the apparent second-order rate constant is less likely to be affected by contributions of k_{micro} that may involve folding processes in the encounter complex.

The association reactions of both the P-22 Arc monomers and the S peptide and S protein exhibit substantial $\Delta C_p^{\circ\ddagger}$ values, −0.9 and −0.7 kcal mol^{-1} K^{-1}, respectively (*11*, *43*). The negative values are consistent with the burial of

hydrophobic surface area in the folding reaction. Unfortunately, the k_{UI} rate constant for $[2-66]_2$ TR was too great to monitor over a sufficiently broad temperature range to accurately determine $\Delta C_p^{\circ\ddagger}$ from plots of ln(k) vs 1/T.

Urea and Temperature Dependence of the Properties of the $I_2 \rightleftharpoons N_2$ Transition State. The values of $m^{\ddagger}$ and $\Delta C_p^{\circ\ddagger}$ are expected to correlate with changes in ΔASA between the initial species and the transition state which links it to the final species in the reaction (*30*, *44*, *45*). In the unfolding reaction, which monitors the changes between N_2 and the transition state, neither of these parameters vary within the urea/temperature matrix. The temperature independence of $m^{\ddagger}_{NI}$ and the urea independence of $\Delta C_p^{\circ\ddagger}_{NI}$ strongly suggest that the unfolding transition state does not shift on the energy surface, relative to the native state, as a function of temperature or urea.

In contrast, the $m^{\ddagger}$ value for the refolding reaction has a marked temperature dependence. The value of $m^{\ddagger}_{NI}$ increases by a factor of ∼2 from 5 to 35 °C, though this change is not monotonic (Figure 4). There is no discernible urea dependence of the $\Delta C_p^{\circ\ddagger}_{NI}$ term. Because the transition state observed in the unfolding reaction does not move on the energy surface, it is likely that the temperature dependence of $m^{\ddagger}_{NI}$ is the result of the movement of I_2 on the energy surface. Presumably, I_2 is somewhat thermally labile and undergoes a transition to a more open form between 10 and 22 °C (Figure 4).

The $N_2 \rightarrow I_2$ unfolding reaction exhibits a urea independent $\Delta S^{\circ\ddagger}$ and a very small urea dependence for $\Delta H^{\circ\ddagger}$ and $\Delta G^{\circ\ddagger}$, −0.16 kcal mol^{-1} M^{-1} (Figure 6). The urea dependence of the $\Delta H^{\circ\ddagger}$ parameter has been proposed to correspond to the enthalpy released or absorbed upon urea binding, $\Delta H^{\circ\ddagger}_{bind}$ (*4*). Urea binding to an unfolded protein has an enthalpy of −2.2 kcal mol^{-1} M^{-1} and an entropy of −12.9 cal mol^{-1} K^{-1} M^{-1} (*46*); similar values of $\Delta H^{\circ\ddagger}_{bind}$ and $\Delta S^{\circ\ddagger}_{bind}$, −2.9 kcal mol^{-1} M^{-1} and −15.4 cal mol^{-1} K^{-1} M^{-1}, respectively, were found for the binding of urea to the transition state in the unfolding of the αTS (*4*). Unlike the values for $\Delta G^{\circ\ddagger}$ and $\Delta S^{\circ\ddagger}$, the urea dependence of these parameters, i.e., $\Delta G^{\circ\ddagger}_{bind}$ and $\Delta S^{\circ\ddagger}_{bind}$, do not depend on the formalism chosen to relate the rate constant to the activation energy. The order of magnitude lower value of $\Delta H^{\circ\ddagger}_{bind}$ for the interaction of urea with the unfolding transition state of $[2-66]_2$ TR suggests that the accessibility of the backbone to urea in the transition state is similar to that in N_2 and that urea is binding in a manner different from that observed for an unfolded protein. A different mechanism of urea binding, such as to side chains, particularly those on the surface (*47*, *48*), may be operative. This interpretation is consistent with the very low ΔASA seen between N_2 and the unfolding transition state. The ratio of the $m^{\ddagger}_{NI}$ and the m value for the complete unfolding of $[2-66]_2$ TR (2.0 kcal mol^{-1} M^{-1}; ref *14*) is 0.088, meaning that less than 10% of the surface area buried in N_2 has been exposed to solvent in the transition state.

In contrast, the values of $\Delta S^{\circ\ddagger}$ and $\Delta H^{\circ\ddagger}$ for the $I_2 \rightarrow N_2$ folding reaction show a strong urea dependence. The values of $\Delta S^{\circ\ddagger}_{bind}$ and $\Delta H^{\circ\ddagger}_{bind}$ are −8.5 ± 0.5 cal mol^{-1} K^{-1} and −1.9 kcal mol^{-1} M^{-1}. These values are similar to those seen for urea binding to unfolded proteins (*46*), suggesting that the backbone is partially nonhelical and exposed to solvent in I_2. The far-UV CD signal of I_2 is ∼30% lower than that of N_2, consistent with this interpretation. Comparison of the enthalpy of urea binding on the folding and unfolding sides of the transition state suggests that most of the denaturant dissociates from I_2 when the transition state to N_2 is reached.

Location of the Transition State with Respect to I_2 and N_2. Insights can be gained from the relative position of the transition state and its similarity to the native species, with respect to buried surface area, by examining the value of α (*44*):

$$\alpha = \frac{X^{\ddagger}_{IN}}{X^{\ddagger}_{IN} - X^{\ddagger}_{NI}} \qquad (9)$$

where X is either the $\Delta C_p^{\circ\ddagger}$ or $m^{\ddagger}$ value. An α value approaching 1 indicates that the transition state is very nativelike; conversely, a value nearer to 0 indicates that the transition state is more like the intermediate. The α value derived from the $m^{\ddagger}$ value is 0.76 at 25 °C (preceding paper in this issue), though it decreases to 0.62 below 10 °C. The α-value, from the $\Delta C_p^{\circ\ddagger}$ values, is substantially smaller, 0.43. The inconsistencies between these two α values presumably arise from the different responses of m and ΔC_p° to the burial of hydrophilic surface area. The values of both parameters are dominated by a positive contribution for the burial of hydrophobic surface area (*49*, *50*). However, there is a small, negative contribution to ΔC_p° from the burial of polar surfaces; in contrast, the sign of the small contribution to the m value from burial of polar surfaces is positive. Thus, the m value reflects the burial of the total surface area, whereas ΔC_p° is modulated by the nature of the buried surface. For protein folding reactions where α values from both $\Delta C_p^{\circ\ddagger}$ and $m^{\ddagger}$ values have been reported, most exhibit a discrepancy between these two values. For example, the $\Delta C_p^{\circ\ddagger}$ α values are lower than those from the $m^{\ddagger}$ value for chymotrypsin inhibitor 2 (*5*, *7*), the Fyn SH3 domain (*9*), and cold shock protein B (*8*).

The α value determined from the urea-dependence of the rate constants for αTS is a more reliable measure of the position of the transition state along the reaction coordinate than that measured from the heat capacity. The $m^{\ddagger}$ values are more accurately determined than the $\Delta C_p^{\circ\ddagger}$ values and are proportional to the total buried surface area. Furthermore, if the I_2 state shifts along the reaction coordinate as proposed, the interpretation of $\Delta C_p^{\circ\ddagger}$ becomes complicated. Therefore, although the α value decreases from 0.76 at 25 °C to 0.62 at 10 °C, the transition state remains relatively nativelike.

Reaction Profile for the Folding of $[2-66]_2$ TR. From the data presented in this paper and the previous reports on the equilibrium and kinetic mechanisms of the folding of $[2-66]_2$ TR (*14*; preceding paper in this issue], it is possible to construct reaction profiles for the folding of this dimeric subdomain (Figure 8). The data are presented at the standard state of 298 K and 0 M urea, except for TS_{IU}, for which data could only be collected at 1.0 M urea (preceding paper in this issue). Because the values of $\Delta S^{\circ\ddagger}$ and $\Delta G^{\circ\ddagger}$ are dependent on the choice of formalism and preexponential factor, the profiles for both the first- and second-order reactions are shown using two limits for the prefactor. An upper limit is given by using the Eyring model, with $k_B T/h$

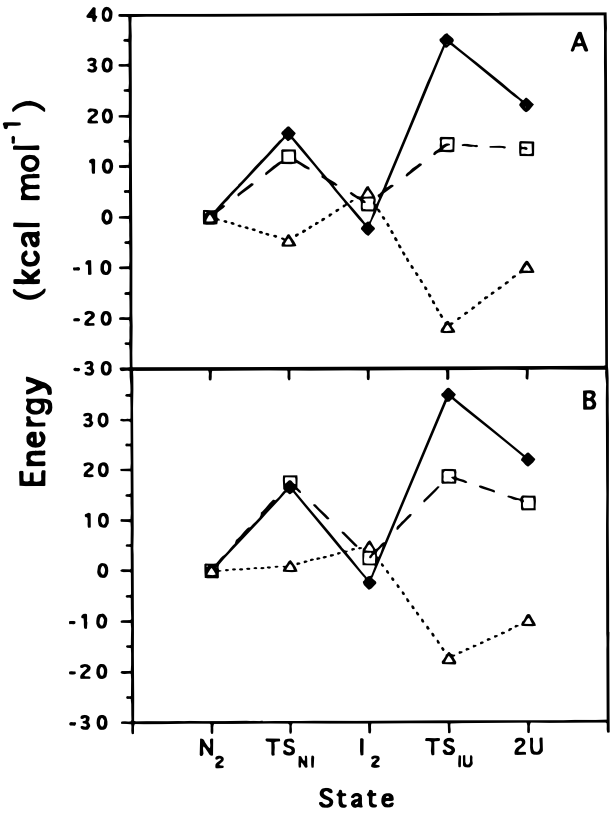

FIGURE 8: Reaction profiles for $[2-66]_2$ TR at a standard state of 298 °C and 0 M urea. N_2 is taken as the reference state, and its properties arbitrarily set to zero. The values of $\Delta G°$ for U were taken from the equilibrium urea-induced unfolding; those for $\Delta H°$ and $\Delta S°$ were calculated from the total change in the three-state thermal denaturation of $[2-66]_2$ TR; i.e., $\Delta X°(U) = \Delta X_{NI}(T=298) + \Delta X_{IU}(T=298)$ (data from ref *14*). The reaction profiles were calculated using both the Kramers formalism, with preexponential factors of 3.3×10^9 M^{-1} s^{-1} and 5×10^8 s^{-1} (panel A), and the Eyring formalism, with a preexponential factor of $k_BT/h = 6.2 \times 10^{12}$ s^{-1} (panel B). $\Delta H°$, which is independent of the prefactor (eq 3), ♦ and —; $-T\Delta S°$, Δ and ⋯; $\Delta G°$, □ and --.

$= 6.2 \times 10^{12}$ s^{-1} (Figure 8B) as the preexponential factor. Alternatively, a lower limit can be employed using the Kramers' model (Figure 8A) with preexponential values of 3.3×10^9 M^{-1} s^{-1} for the second-order reaction and 5×10^8 s^{-1} for the first-order reaction, as estimated from peptide models that yielded values of $(3-8) \times 10^8$ s^{-1} (*28*, *29*).

For both the NI and IU transition states, using either formalism, the barriers are dominated by enthalpic contributions. Particularly for the second-order step, the entropic contribution lowers the free energy of the barrier, accelerating the reaction. Entropy also mediates the overall reaction from I_2 to N_2, which actually has a slightly unfavorable enthalpy change. The driving force is the opposite for the 2U to I_2 reaction, where the loss of ~50 eu is more than compensated for by an enthalpy gain of ~24 kcal mol^{-1}.

Summary. The transition-state analyses described herein elucidate the dominant role of enthalpy in retarding both subunit association and subsequent rearrangement reactions in the folding of $[2-66]_2$ TR. The magnitude and sign of the entropic components reflect the interplay between the loss of entropy of the polypeptide and gain of entropy for the solvent in the folding reaction; the latter is the predominant effect in accelerating the association reaction. The data also highlight the often opposing contributions of enthalpy and entropy in determining the free energy surface that describes the folding of $[2-66]_2$ TR.

ACKNOWLEDGMENT

The global fitting program used in this work, Savuka 5.0, was written by Dr. Osman Bilsel. We are grateful for his development of this program and his assistance in its utilization.

REFERENCES

1. Baldwin, R. L., and Roder, H. (1991) *Curr. Biol. 1*, 218−220.
2. Matthews, C. R. (1993) *Ann. Rev. Biochem. 62*, 653−683.
3. Chen, B.-L., Baase, W. A., and Schellman, J. A. (1989) *Biochemistry 28*, 691−699.
4. Chen, X., and Matthews, R. (1994) *Biochemistry 33*, 6356−6362.
5. Jackson, S. E., and Fersht, A. R. (1991) *Biochemistry 30*, 10436−10443.
6. Oliveberg, M., and Fersht, A. R. (1996) *Biochemistry 35*, 2738−2749.
7. Tan, Y.-J., Oliveberg, M., and Fersht, A. R. (1996) *J. Mol. Biol. 264*, 377−389.
8. Schindler, T., and Schmid, F. X. (1996) *Biochemistry 35*, 16833−16842.
9. Plaxco, K. W., et al. (1998) *Biochemistry 37*, 2529−2537.
10. Parker, M. J., Lorch, M., Sessions, R. B., and Clarke, A. R. (1998) *Biochemistry 37*, 2538−45.
11. Milla, M. E., and Sauer, R. T. (1994) *Biochemistry 33*, 1125−1133.
12. Zhang, R.-G., et al. (1987) *Nature 327*, 591−597.
13. Zhao, D., Arrowsmith, C. H., Jia, X., and Jardetzky, O. (1993) *J. Mol. Biol. 229*, 735−746.
14. Gloss, L. M., and Matthews, C. R. (1997) *Biochemistry 36*, 5612−5623.
15. Gittelman, M. S., and Matthews, C. R. (1990) *Biochemistry 29*, 7011−7020.
16. Mann, C. J., Xiao, S., and Matthews, C. R. (1995) *Biochemistry 34*, 14573−14580.
17. Zitzewitz, J. A., Bilsel, O., Luo, J., Jones, B. E., and Matthews, C. R. (1995) *Biochemistry 34*, 12812−12819.
18. Bernasconi, C. F. (1976) *Relaxation Kinetics*, Academic Press, New York.
19. Press, W. H., Flannery, B. P., Teukolsky, S. A., and Vetterling, W. (1989) *Numerical Recipes: The Art of Scientific Computing (FORTRAN vesion)*, Cambridge University Press, Cambridge, U.K.
20. Amdur, I., and Hammes, G. G. (1966) *Chemical Kinetics: Principles and Selected Topics*, McGraw-Hill, New York.
21. Atkins, P. W. (1986) *Physical Chemistry*, Freeman and Co., New York.
22. Glasstone, S., Laidler, K. J., and Eyring, H. (1940) *Theory of Rate Processes*, McGraw-Hill, New York.
23. Kramers, H. A. (1940) *Physica 7*, 284.
24. Beasty, A. M., and Matthews, C. R. (1985) *Biochemistry 24*, 3547−3553.
25. Berg, O. G., and von Hippel, P. H. (1985) *Annu. Rev. Biophys. Biophys. Chem. 14*, 131−160.
26. Janin, J. (1997) *Proteins 28*, 153−161.
27. Chen, B.-L., and Schellman, J. A. (1989) *Biochemistry 28*, 685−691.
28. Thompson, P. A., Eaton, W. A., and Hofrichter, J. (1997) *Biochemistry 36*, 9200−9210.
29. Munoz, V., Henry, E. R., Hofrichter, J., and Eaton, W. A. (1998) *Proc. Natl. Acad. Sci. U.S.A. 95*, 5872−5879.
30. Myers, J. K., Pace, C. N., and Scholtz, J. M. (1995) *Protein Sci. 4*, 2138−2148.
31. Socci, N. D., Onuchic, J. N., and Wolynes, P. G. (1996) *J. Chem. Phys. 104*, 5860−5868.
32. Eaton, W. A., Munoz, V., Thompson, P. A., Chan, C.-K., and Hofrichter, J. (1997) *Curr. Opin. Struct. Biol. 7*, 10−14.

33. Mann, C. J., and Matthews, C. R. (1993) *Biochemistry 32*, 5282−5290.
34. Shao, X., Hensley, P., and Matthews, C. R. (1997) *Biochemistry 36*, 9941−9949.
35. Weast, R. C., Ed. (1984) *CRC Handbook of Chemistry and Physics*, CRC Press, Inc., Boca Raton, FL.
36. Makhatadze, G. I., and Privalov, P. L. (1993) *J. Mol. Biol. 232*, 639−659.
37. D'Aquino, J. A., et al. (1996) *Proteins 25*, 143−156.
38. Privalov, P. L., and Makhatadze, G. I. (1993) *J. Mol. Biol. 232*, 660−679.
39. Laurents, D. V., and Baldwin, R. L. (1998) *Biophys. J. 75*, 428−434.
40. Israelachvili, J., and Pashley, R. (1982) *Nature 300*, 341−342.
41. Tsao, Y.-H., Evans, D. F., and Wennerström, H. (1993) *Science 262*, 547−550.
42. Goldberg, J. M., and Baldwin, R. L. (1998) *Biochemistry 37*, 2546−2555.
43. Goldberg, J. M., and Baldwin, R. L. (1998) *Biochemistry 37*, 2556−2563.
44. Tanford, C. (1970) *Adv. Protein Chem. 24*, 1−95.
45. Schellman, J. A. (1978) *Biopolymers 17*, 1305−1322.
46. Makhatadze, G. I. and Privalov, P. L. (1992) *J. Mol. Biol. 226*, 491−505.
47. Hibbard, L. S. and Tulinsky, A. (1978) *Biochemistry 17*, 5460−5468.
48. Dunbar, J., Yennawar, H. P., Banerjee, S., Luo, J., and Farber, G. K. (1997) *Protein Sci. 6*, 1727−1733.
49. Privalov, P. L., and Makhatadze, G. I. (1992) *J. Mol. Biol. 224*, 715−723.
50. Murphy, K. P., and Freire, E. (1992) *Adv. Protein Chem. 43*, 313−361.
51. Kraulis, P. J. (1991) *J. Appl. Crystallogr. 24*, 946−950.
52. Gloss, L. M., and Matthews C. R. (unpublished results).
53. Shao, X., and Matthews, C. R. (unpublished data).

BI981694F